The Astrophysical Journal, 622:1102–1117, 2005 April 1

THE PLANET-METALLICITY CORRELATION[1]

Debra A. Fischer[2] and Jeff Valenti[3]

Received 2004 October 4; accepted 2004 December 3

ABSTRACT

We have recently carried out spectral synthesis modeling to determine $T_{\rm eff}$, $\log g$, $v \sin i$, and [Fe/H] for 1040 FGK-type stars on the Keck, Lick, and Anglo-Australian Telescope planet search programs. This is the first time that a single, uniform spectroscopic analysis has been made for every star on a large Doppler planet search survey. We identify a subset of 850 stars that have Doppler observations sufficient to detect uniformly all planets with radial velocity semiamplitudes $K > 30$ m s^{-1} and orbital periods shorter than 4 yr. From this subset of stars, we determine that fewer than 3% of stars with $-0.5 <$ [Fe/H] < 0.0 have Doppler-detected planets. Above solar metallicity, there is a smooth and rapid rise in the fraction of stars with planets. At [Fe/H] $> +0.3$ dex, 25% of observed stars have detected gas giant planets. A power-law fit to these data relates the formation probability for gas giant planets to the square of the number of metal atoms. High stellar metallicity also appears to be correlated with the presence of multiple-planet systems and with the total detected planet mass. This data set was examined to better understand the origin of high metallicity in stars with planets. None of the expected fossil signatures of accretion are observed in stars with planets relative to the general sample: (1) metallicity does not appear to increase as the mass of the convective envelopes decreases, (2) subgiants with planets do not show dilution of metallicity, (3) no abundance variations for Na, Si, Ti, or Ni are found as a function of condensation temperature, and (4) no correlations between metallicity and orbital period or eccentricity could be identified. We conclude that stars with extrasolar planets do not have an accretion signature that distinguishes them from other stars; more likely, they are simply born in higher metallicity molecular clouds.

Subject headings: planetary systems — stars: abundances — stars: fundamental parameters

Online material: machine-readable tables

1. INTRODUCTION

The detection of extrasolar planets has garnered tremendous public and scientific interest and launched a new subfield in astronomy. While photons from the planets themselves still elude detection, the bright host stars are accessible to even modest-sized telescopes armed with high-resolution spectrometers. As a result, there have been numerous investigations of the chemical abundances of host stars with the goal of better understanding the conditions that lead to planet formation. These spectroscopic studies have demonstrated that stars with extrasolar planets tend to have a higher metallicity than stars without detected extrasolar planets.

The physical mechanism for the observed planet-metallicity correlation is of particular interest. One explanation posits that high metallicity enhances planet formation because of increased availability of small particle condensates, the building blocks of planetesimals. Alternatively, enhanced stellar metallicity may be a by-product of late-stage accretion of gas-depleted material, so-called pollution of the convective zone (CZ) of the star. These two mechanisms leave different marks on the host stars; in the first case, a high-metallicity protostellar cloud forms a star that is metal-rich throughout. However, in the latter case, high metallicity is confined to the stellar CZ and the interior of the star is left with lower metallicity.

Gonzalez (1997) published a seminal paper measuring relatively high stellar metallicity in host stars of the first four detected extrasolar planets. He attributed this correlation to the accretion of gas-depleted material, as described by Lin et al. (1996). Of particular note, Gonzalez highlighted the importance of CZ mass, which serves as the diluting medium for accreted material. F dwarfs with relatively thin CZs will exhibit a greater degree of pollution than G dwarfs for a fixed amount of accreted material. Therefore, a telltale signature of accretion would be a metallicity distribution where the upper boundary in the metallicity of F dwarfs exceeds the highest metallicity observed in G dwarfs. Gonzalez extended his discussion of the importance of CZ mass, noting that as stars evolve, their enriched convective envelopes would be diluted by deeper, unenriched layers, and the high-metallicity accretion signature would be lost. Finally, Gonzalez noted that accretion of fractionated material by Poynting-Robertson drag or by accretion of cometary material could leave an important signature: a correlation between elemental abundances and their condensation temperatures. These testable predictions focused the direction of subsequent theoretical predictions and spectroscopic investigations.

Lin et al. (1996) proposed that gas giant planets in short-period orbits (like 51 Peg b) formed at wider separations and migrated inward. They pointed out that close-in planets were likely to be the tail of a stream of planets and disk material that accreted onto the surface of the star and mixed in the stellar CZ, enriching the observed stellar metallicity. Laughlin & Adams (1997) quantified the expected elevation in stellar metallicity by accretion of Jupiter-like planets that migrate into the CZ during pre–main-sequence disk lifetimes. Their simulations demonstrated that accretion of planets at this stage would produce a detectable metallicity enhancement only in earlier type stars, such as F dwarfs. They suggested that the metallicity signature would be more clearly associated with stellar mass than with effective

[1] Based on observations obtained at Lick and Keck Observatories, operated by the University of California, and the Anglo-Australian Observatories.

[2] Department of Physics and Astronomy, San Francisco State University, 1600 Holloway, San Francisco, CA 94132; fischer@stars.sfsu.edu.

[3] Space Telescope Science Institute, 3700 San Martin Drive, Baltimore, MD.

temperature. Examining literature abundance values, they found that while a trend in metallicity with stellar mass was plausible, higher precision abundances for a large sample of stars were needed to draw any firm conclusions.

Pinsonneault et al. (2001) questioned the existence of an accretion signature after modeling the increase in metallicity arising from accretion of $\sim$10 $M_{\rm earth}$ of material onto zero-age main-sequence stars. Their models show that accretion of $\sim$10 $M_{\rm earth}$ of gas-depleted material would elevate the metallicity of solar-metallicity G dwarfs to [Fe/H] $\sim$ 0.3. However, this same accretion mass would result in another factor of 2 increase in metallicity in an F dwarf to [Fe/H] $\sim$ 0.6. These models emphasize an expected telltale signature of accretion: the observed upper boundary in a metallicity distribution should increase as the CZ thickness decreases.

A mechanism that might soften or obscure differences in accretion pollution levels between F and G type stars was proposed by Sandquist et al. (1998). While their models also show that CZ thickness is an important factor in the level of metallicity enhancement from accretion of Jovian planets, they offer a caveat: thinner CZs may be less effective at stripping mass from accreted planets, so much of the planet core may pass unperturbed through the CZ. Furthermore, if a metallicity gradient exists in the accreted planet, with most of the heavy elements in the planet core, then even fewer heavy metals would be deposited in the stellar CZ and metallicity may not be noticeably increased for earlier type stars. This work essentially proposes the possibility of a self-regulating process for stars that swallow Jovian-mass planets. If such a process takes place, then the upper envelope of the metallicity distribution could be flat, declining, or simply rising more slowly than predicted as the CZ thickness decreases.

Murray et al. (2001) suggest a clever scheme that utilizes observations of lithium abundances to empirically establish the mixing depth of the CZ. Their idea makes use of the fact that the temperature at the base of the CZ sets the lithium depletion timescale. Stars with thick CZs, such as G dwarfs, destroy lithium on timescales of a few hundred million years. However, the CZ thins with increasing stellar mass and in late F-type stars, the thin CZ is held farther away from lithium-destroying temperatures. There lithium survives for a few billion years. A surprising reversal in this trend takes place as the stellar mass approaches 1.4 $M_{\odot}$ and the lithium abundance suddenly plummets. This so-called lithium dip presumably occurs because of the onset of an extra mixing mechanism. Murray et al. postulate that a parallel trend should be observed with iron abundances in F-type stars: there should be a peak in metallicity near 1.2 $M_{\odot}$ followed by a drop in metallicity near 1.4 $M_{\odot}$.

Spectroscopic abundance analysis papers of planet-bearing stars raced alongside theory and extrasolar planet discovery papers (Fuhrmann et al. 1997, 1998; Gonzalez 1998, 1999; Gonzalez et al. 2001; Santos et al. 2000, 2003, 2004; Sadakane et al. 2002; Laws et al. 2003). These spectral analyses generally compare metallicities for subsets of planet-bearing stars with metallicity distributions for volume-limited samples, often determined by other researchers using a different abundance analysis technique. The validity of such comparisons faces a couple of serious challenges. First, systematic offsets in spectroscopically derived parameters by different researchers are common, and the magnitude of the proposed metallicity correlation is comparable to systematic offsets and typical errors in most abundance analyses. Second, the stars on planet search surveys are not necessarily drawn from the same parent population as the adopted comparison samples. If the stars on Doppler surveys have higher metallicity than a typical volume-limited sample, then this would certainly result in a metallicity correlation but not a physically meaningful one.

While stars with detected planets have been carefully scrutinized, the properties of all other stars on Doppler surveys (without detected planets) have not yet been examined with a single, uniform technique. Together with a companion paper, Valenti & Fischer (2005, hereafter VF05), we present results from a high-resolution spectroscopic analysis employing a single technique to derive $T_{\rm eff}$, abundances, surface gravity, and $v \sin i$ for every FGK type star on the Keck, Lick, and Anglo-Australian Telescope (AAT) planet search surveys. A description of the spectroscopic analysis technique and the derived parameters for 1040 stars are given in VF05. In this paper, we examine metallicity distributions for several different stellar samples, namely, the three planet search samples, the planet-bearing stars, a volume-limited subset of stars, and a set of 86 subgiants, to qualify and quantify the planet-metallicity correlation. We also include spectral analysis results for a few additional planet-bearing stars on other Doppler surveys to obtain a nearly complete table of characteristics of stars with detected extrasolar planets.

2. THE SPECTRAL ANALYSIS TECHNIQUE

A detailed description of the methodology and an assessment of random and systematic errors is provided in VF05. In brief, our spectral modeling program, SME (VF05; Valenti & Piskunov 1996), assumes local thermodynamic equilibrium and drives a radiative transfer code using Kurucz stellar atmosphere models (Kurucz 1993) and atomic line data (Vienna Atomic Line Database [VALD]; Kupka et al. 1999; Ryabchikova et al. 1999) to create a synthetic spectrum. The code employs a nonlinear least-squares Marquardt fitting algorithm to vary free parameters ($T_{\rm eff}$, $\log g$, $v \sin i$, and abundances) in order to best match continuum and spectral line profiles in selected wavelength regions of an observed spectrum. With each Marquardt iteration, the SME program interpolates over a grid of 8000 Kurucz stellar atmosphere models before generating a new synthetic spectrum.

Wavelength segments between 6000 and 6200 Å were selected for our analysis. This "sweet spot" in the solar spectrum is blueward of telluric contamination and redward of heavy spectral line blending, which simplifies continuum placement and minimizes problems with line blending. An additional wavelength segment 5175–5190 Å was included to leverage the gravity sensitivity of the Mg I b triplet lines. Before analyzing our program stars, small adjustments were made to obtain astrophysical atomic line parameters ($\log gf$ values, wavelength shifts, and van der Waal broadening coefficients) by fitting to the high-resolution National Solar Observatory spectrum (Kurucz et al. 1984). After adjusting the atomic line data, several observations of Vesta were analyzed with the SME pipeline. The Vesta analysis returned solar parameters with small systematic offsets (23 K in $T_{\rm eff}$, 0.007 dex in abundance, 0.072 dex in $\log g$) that were eventually applied as corrections to all of the program stars.

Altogether, the modeled wavelength segments contain several hundred neutral and ionized atomic lines that span a range of excitation potentials. In many cases, these spectral lines respond in opposing ways to changes in stellar parameters, so that collectively, this ensemble of lines helps to break degeneracy when simultaneously fitting $T_{\rm eff}$, abundances, and $\log g$. More than 300 MgH and C_2 lines were also modeled because the Mg I b lines, critical for an assessment of surface gravity, are blanketed with these molecular lines. Our study is confined to stars with $T_{\rm eff} > 4700$ K where atmospheric models and our analysis are robust.

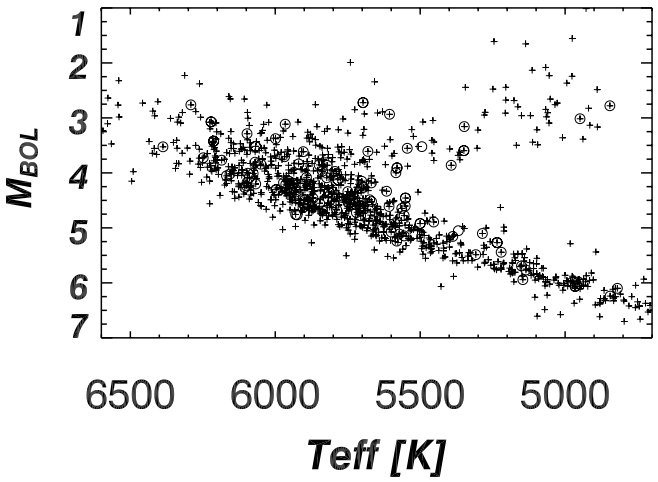

FIG. 1.—H-R diagram for stars on the Keck, Lick, and AAT planet search projects using SME-derived effective temperatures and absolute bolometric magnitudes. The uncertainties in $T_{\rm eff}$ are about 1%. Plus signs represent stars in the general sample (see VF05 for these data), and stars with detected extrasolar planets are circled.

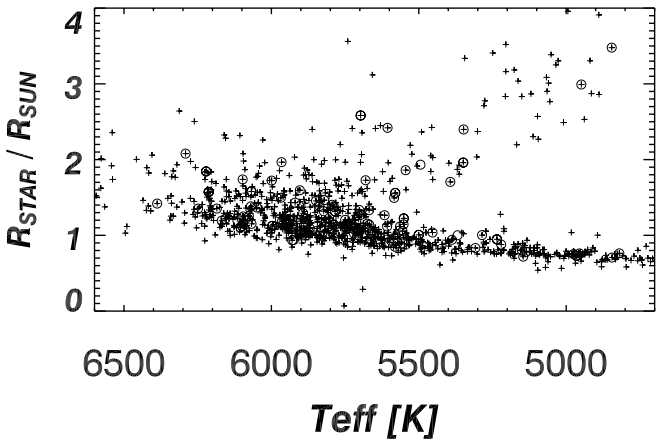

FIG. 2.—Stellar radii for the entire Keck, Lick, and AAT planet search samples (*plus signs*) and for stars with known planets (*circles*) are plotted against SME-derived $T_{\rm eff}$. Uncertainties in the stellar radii are on the order of a few percent.

2.1. *The Stellar Sample*

We have carried out spectral synthesis modeling for 1040 stars observed at Keck Observatory, Lick Observatory, and the Anglo-Australian Observatory as part of the California & Carnegie and the Anglo-Australian planet search projects. The stars for these surveys are selected to optimize the achievable Doppler velocity precision and so favor bright, chromospherically inactive, main-sequence or subgiant stars ($M_V > 3.0$, $V < 8.5$, and $B - V > 0.5$). As part of the Doppler analysis (Butler et al. 1996) a template spectrum with S/N $\sim$ 300 is obtained for each star. These spectra have a resolution of $\sim$90,000 with the Hamilton spectrograph at Lick Observatory, $\sim$70,000 with HIRES at Keck Observatory, and $\sim$70,000 with UCLES at the Anglo-Australian Observatory. We make serendipitous use of these high-quality template spectra to carry out a uniform abundance analysis of more than 1900 template spectra from these three observatories.

As discussed in VF05, our 1 σ uncertainties are about $\pm$44 K for $T_{\rm eff}$, $\pm$0.06 dex for log g, $\pm$0.03 dex for abundances, and $\pm$0.5 km s^{-1} for $v \sin i$. A number of researchers have carried out spectroscopic analyses for smaller subsets of stars in common with our sample. In VF05, our results are compared with published stellar parameters. Effective temperatures and abundances show excellent agreement with these published results; however, small systematic offsets are apparent. A comparison of log g values shows larger rms scatter, but they generally agree within quoted ($\sim$0.15 dex) uncertainties. While different spectroscopic analyses show reasonable agreement, the nonnegligible systematic offsets demonstrate that spectroscopic results from different investigators should be combined with caution, particularly when looking for subtle correlations or trends.

Figure 1 shows an H-R diagram of stars in the planet search programs, with absolute bolometric magnitude plotted against our derived effective temperatures. Throughout this paper, plus signs represent stars on the planet search samples, and circles designate stars known to harbor planets. From Figure 1, it is clear that stars with detected planets span the main sequence and infiltrate the subgiant branch. Planet-bearing stars appear to edge toward the top of the main-sequence distribution, typical of high-metallicity stars, which move diagonally on an H-R diagram to slightly lower luminosity and cooler effective temperatures.

We combine stellar luminosities derived with *Hipparcos* parallaxes and a bolometric correction (VandenBerg & Clem 2003) with our measured $T_{\rm eff}$ to calculate radii for our stars ($L = 4\pi R^2 \sigma T_{\rm eff}^4$), with a median error of 3%. Figure 2 shows stellar radii as a function of $T_{\rm eff}$ for all stars on the Keck, Lick, and AAT projects. Planet-bearing stars are again circled. The tight distribution of data points in this diagram reflects the small uncertainties in the constituent parameters, $T_{\rm eff}$ and R_*. Stars with detected planets appear to be representative of the overall survey sample. It is straightforward to combine stellar radii and our measured log g values to calculate stellar masses:

$$M_* = \frac{gR^2}{G}.$$

The uncertainties in these stellar masses are dominated by errors in the measured gravities. For stars that are about 1 $M_\odot$, our uncertainty of 0.06 dex in log g translates to $\sim$15% uncertainties in stellar mass. However, the measurement of log g is challenging, in part because of degeneracy in the global solution between log g and $T_{\rm eff}$ and (to a lesser extent) with [Fe/H]. As an independent assessment of the accuracy of the calculated stellar masses, we derived masses from stellar isochrones. Hillenbrand & White (2004) find the best agreement between dynamical masses (particularly for low-mass stars) and Y^2 models from the Yale group (Yi et al. 2003). We use *Hipparcos*-based stellar luminosities, together with our SME-measured $T_{\rm eff}$ and [Fe/H], and interpolate over a grid of Y^2 stellar evolution models. The model stellar masses are accurate to about $\sim$10% in a relative sense, although uncertainties in the observed parameters used to identify the position on the isochrones introduce additional random errors. A comparison of the model stellar masses with our calculated stellar masses allows us to identify stars that are likely to have excessive errors in log g. In general, the model-derived masses appear to be more reliable and are adopted in all further discussions and in our analysis. Stellar masses for all stars are plotted in Figure 3, and a representation of a 10% error bar in the model masses is provided in the lower left corner of the plot.

2.2. *Stellar Parameters for Stars with Planets*

Currently, planets have been discovered around 117 stars; 11 of these stars harbor double-planet systems, two are triple-planet systems, and one has four detected planets, bringing the total

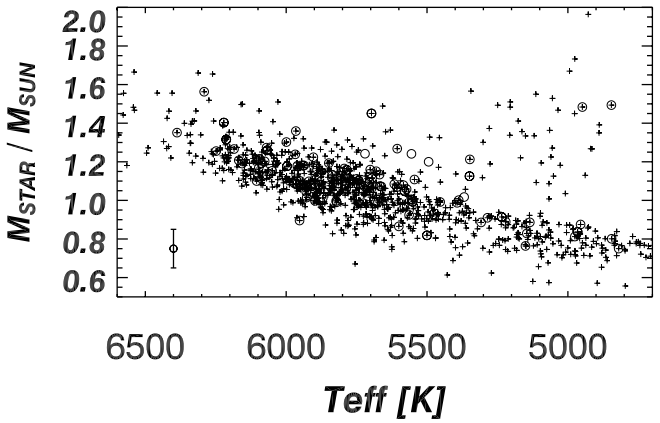

FIG. 3.—Stellar masses are derived from Yale isochrones for all planet search stars and for stars with known planets using the same symbols as Fig. 2. A representative 10% error bar is shown that is typical for the model stellar masses.

number of detected exoplanets to 135. We have carried out spectroscopic analysis for 105 of these planet-bearing stars. We have not yet analyzed M dwarfs (GJ 876 or GJ 436) or evolved Class III stars (HD 219499, HD 104985, HD 59686, and HD 137759), and spectra were unavailable for HD 330075, HD 6434, HD 121504, HD 65215, and HD 41004.

The measured and derived parameters for 105 stars with known planets are listed in Table 1, including $T_{\rm eff}$, $\log g$, elemental abundances for [Na/H], [Ti/H], [Si/H], [Fe/H], and [Ni/H], and $v \sin i$. (Most of these values were provided in VF05.) Table 1 also lists the observatory where spectra were obtained (K = Keck, A = AAT, L = Lick), the number of spectra analyzed, and the derived stellar mass and radii. Table 2 lists the number of detected planets ($N_{\rm pl}$), the orbital period in days, the velocity semiamplitude, orbital eccentricity, companion mass times the unknown orbital inclination ($M \sin i$), the semimajor axis of the planet orbit relative to the star ($a_{\rm rel}$), and the publication year of the detection paper.

3. EXAMINING THE METALLICITY CORRELATION

We propose that the best way to understand the correlation between metallicity and extrasolar planets is to start with a uniform analysis of all of the stars and then ask the straightforward question: What fraction of stars in each metallicity bin have planets?

Even though the metallicity analysis is carried out in a uniform manner, planet detectability will still vary because the frequency and duration of Doppler observations is different for each star. However, most stars on the planet search programs have nearly uniform detectability for companions with velocity amplitudes $K > 30$ m s^{-1} and orbital periods shorter than 4 yr. A subset of SME-analyzed stars was selected that had at least 10 observations spanning four or more years. This restriction for nearly uniform planet detectability was met for 850 of 1040 SME-analyzed stars. In fact, most of the 850 stars have many more observations, spanning several years. We also required that all stars were independently selected targets for the Keck, Lick, and AAT surveys; stars that were added after a planet was discovered by another group were not included in our statistical count. However, stars independently present on our survey were counted even if a planet was detected first by another group. Only planets with $K > 30$ m s^{-1} and orbital periods shorter than 4 yr were included in our statistical count. This corresponds to Saturn-mass planets for the shortest period orbits and Jupiter-mass planets in 4 yr orbits.

The subset of 850 FGK-type stars with both uniform abundance analysis and uniform planet detectability were binned according to metallicity. The Doppler velocities for every star were reviewed to determine the fraction of stars in each metallicity bin with a planet that had $K > 30$ m s^{-1} and an orbital period of 4 yr or less. The set of stars used for this statistical count is listed in Table 3 (complete list in the electronic version only). In this table, the star identifier is given that matches the star identifier provided in VF05. A flag in the table indicates whether that star has a known planet ("P") or is a star without a detected planet ("S"). In Figure 4, the stars are divided into 0.25 dex bins. The ratio of planet-bearing stars to all stars in the bin is labeled above each metallicity bin and error bars are calculated assuming Poisson statistics (i.e., the percentage of stars with planets divided by the square root of the number of planets). This same analysis was presented at a somewhat earlier stage (Fischer et al. 2004) one year ago. Since that time, all spectral models were rerun with an improved formulation for macroturbulent velocity and $\log g$ was added as a free parameter in the fit. An additional $\sim$200 stars and a dozen new planets have met the uniform detectability threshold in the past year. Despite the changes in our spectroscopic analysis and the additions to the sample, the quantification of planet occurrence with stellar metallicity has not changed; the percentage of stars with planets agrees with our earlier analysis within error bars for each of the 0.25 dex metallicity bins, as expected for a statistically robust analysis.

To investigate the metallicity correlation in more detail, we divided the stars into finer 0.1 dex metallicity bins. Figure 5 shows a smooth, continuous increase in the fraction of stars with planets as a function of increasing metallicity above [Fe/H] = 0.0. Fewer than 3% of stars with subsolar metallicity have detected planets, but 25% of stars with [Fe/H] > 0.3 dex have detected planets. Santos et al. (2003) originally quantified a 7% planet occurrence in this highest metallicity bin, but in a revised analysis (Santos et al. 2004) they now concur with Fischer et al. (2004) that 25%–30% of the highest metallicity stars on the Geneva planet search survey have detected gas giant planets.

The relationship shown in Figure 5 quantifies the probability, $\mathcal{P}$(planet), of formation of a gas giant planet with orbital period shorter than 4 yr and $K > 30$ m s^{-1} as a function of metallicity. This correlation applies to FGK-type main-sequence stars and is valid over the metallicity range $-0.5 <$ [Fe/H] < 0.5:

$$\mathcal{P}(\text{planet}) = 0.03 \times 10^{2.0[\text{Fe/H}]}.$$

Since $[\text{Fe/H}] = \log (N_{\rm Fe}/N_{\rm H}) - \log (N_{\rm Fe}/N_{\rm H})_{\odot}$, the correlation between planet occurrence and metallicity can be expressed as a power law:

$$\mathcal{P}(\text{planet}) = 0.03 \left[\frac{N_{\rm Fe}/N_{\rm H}}{(N_{\rm Fe}/N_{\rm H})_{\odot}}\right]^2.$$

Thus, the probability of forming a gas giant planet is nearly proportional to the square of the number of iron atoms. It is intriguing that particle collision rates are similarly proportional to the square of the number of particles. This result suggests a physical link between dust particle collision rates in the primordial disk and the formation rate of gas giant planets. This lends further weight to the argument that high metallicity in planet-bearing stars is inherited from the primordial cloud, rather than an acquired asset, and that gas giant planets form by accretion rather than gravitational instabilities in a gaseous disk.

TABLE 1

Derived Parameters for Stars with Planets

Star ID	$T_{\rm eff}$ (K)	$\log g$ (cm s^{-2})	[Fe/H]	[Si/H]	[Ti/H]	[Na/H]	[Ni/H]	$v \sin i$ (km s^{-1})	Site	$N_{\rm obs}$	M_* ($M_\odot$)	R_* ($R_\odot$)
BD −10 3166	5393	4.69	0.38	0.38	0.26	0.50	0.39	0.92	K	1	0.99	1.71
HD 142	6248	4.19	0.10	0.10	0.07	0.07	0.04	10.35	A	6	1.26	1.35
HD 1237	5580	4.56	0.17	0.31	0.09	0.13	0.13	5.03	K	1	0.97	0.85
HD 2039	5940	4.38	0.32	0.33	0.25	0.41	0.34	3.25	A	4	1.18	1.21
HD 3651	5220	4.45	0.16	0.13	0.11	0.24	0.16	1.15	KL	3	0.89	0.88
HD 4203	5701	4.36	0.45	0.40	0.40	0.50	0.47	1.23	K	1	1.16	1.33
HD 4208	5600	4.52	−0.28	−0.21	−0.23	−0.27	−0.31	0.00	K	1	0.87	0.90
HD 8574	6049	4.20	−0.01	−0.00	0.04	−0.03	−0.03	4.52	K	1	1.15	1.37
HD 9826	6212	4.25	0.15	0.17	0.17	0.15	0.13	9.62	L	4	1.32	1.57
HD 10647	6104	4.34	−0.08	−0.08	−0.11	−0.18	−0.15	5.61	A	3	1.10	1.10
HD 10697	5680	4.12	0.19	0.13	0.15	0.17	0.17	2.48	K	1	1.15	1.73
HD 12661	5742	4.42	0.36	0.35	0.32	0.51	0.42	1.30	K	1	1.10	1.12
HD 13445	5150	4.59	−0.27	−0.16	−0.17	−0.24	−0.28	2.37	A	3	0.76	0.80
HD 16141	5793	4.22	0.17	0.11	0.15	0.08	0.14	1.93	K	1	1.17	1.40
HD 17051	6097	4.34	0.11	0.10	0.07	0.08	0.07	6.47	A	3	1.17	1.16
HD 20367	5971	4.31	0.08	0.20	0.05	−0.08	−0.02	3.58	K	1	1.09	1.21
HD 22049	5145	4.57	−0.03	−0.12	−0.05	−0.12	−0.11	2.45	L	2	0.83	0.72
HD 23079	5927	4.34	−0.15	−0.11	−0.06	−0.21	−0.19	2.99	A	5	1.01	1.13
HD 23596	5903	3.97	0.22	0.21	0.15	0.33	0.27	4.22	K	1	1.22	1.60
HD 27442	4845	3.78	0.42	0.28	0.17	0.43	0.50	2.80	A	3	1.49	3.48
HD 28185	5720	4.51	0.24	0.42	0.19	0.38	0.28	1.82	K	1	1.24	1.03
HD 30177	5607	4.31	0.39	0.38	0.30	0.52	0.46	2.96	A	2	1.07	1.12
HD 33636	5904	4.43	−0.13	−0.09	−0.08	−0.22	−0.19	3.08	K	1	1.02	1.00
HD 34445	5836	4.21	0.14	0.12	0.12	0.18	0.14	2.65	K	1	1.11	1.39
HD 37124	5500	4.60	−0.44	−0.21	−0.18	−0.33	−0.40	1.22	K	1	0.82	1.01
HD 38529	5697	4.05	0.45	0.36	0.36	0.51	0.45	3.90	K	1	1.45	2.58
HD 39091	5949	4.36	0.05	0.07	0.02	0.05	0.05	3.14	A	3	1.10	1.15
HD 40979	6089	4.30	0.17	0.16	0.12	0.15	0.14	7.43	K	1	1.19	1.21
HD 45350	5616	4.32	0.29	0.27	0.24	0.27	0.26	1.37	K	1	1.08	1.27
HD 46375	5285	4.53	0.24	0.25	0.22	0.36	0.28	0.86	K	1	0.91	1.00
HD 49674	5662	4.56	0.31	0.27	0.25	0.29	0.30	0.42	K	1	1.07	0.94
HD 50499	6069	4.37	0.34	0.32	0.30	0.42	0.37	4.21	K	1	1.27	1.38
HD 50554	5928	4.29	−0.07	−0.05	−0.05	−0.12	−0.12	3.88	K	1	1.04	1.15
HD 52265	6076	4.26	0.19	0.18	0.20	0.19	0.19	4.67	K	1	1.20	1.25
HD 68988	5960	4.41	0.32	0.34	0.32	0.48	0.39	2.84	K	1	1.18	1.14
HD 70642	5705	4.43	0.16	0.19	0.13	0.29	0.21	0.30	A	6	1.05	1.00
HD 72659	5919	4.24	−0.00	−0.01	0.05	−0.02	−0.02	2.21	K	1	1.10	1.43
HD 73256	5555	4.63	0.28	0.45	0.17	0.33	0.28	3.56	K	1	1.24	0.90
HD 73526	5583	4.16	0.25	0.26	0.27	0.25	0.29	2.62	A	3	1.08	1.49
HD 74156	6067	4.26	0.13	0.10	0.14	0.11	0.13	4.32	K	1	1.26	1.58
HD 75289	6095	4.33	0.22	0.22	0.19	0.14	0.22	4.14	A	3	1.22	1.25
HD 75732	5234	4.45	0.31	0.33	0.23	0.49	0.37	2.46	KL	9	0.91	0.95
HD 76700	5668	4.30	0.35	0.33	0.30	0.35	0.37	1.35	A	6	1.13	1.33
HD 80606	5572	4.44	0.34	0.32	0.21	0.47	0.36	1.80	K	1	1.06	0.90
HD 82943	5997	4.42	0.27	0.24	0.23	0.28	0.29	1.35	K	1	1.18	1.12
HD 83443	5453	4.49	0.36	0.39	0.28	0.57	0.44	1.28	KA	4	0.99	1.04
HD 88133	5494	4.23	0.35	0.49	0.29	0.36	0.42	2.17	K	1	1.20	1.93
HD 89307	5897	4.34	−0.16	−0.12	−0.12	−0.19	−0.19	2.88	K	1	1.00	1.07
HD 89744	6291	4.07	0.26	0.22	0.29	0.26	0.23	9.51	L	3	1.56	2.08
HD 92788	5836	4.66	0.32	0.30	0.29	0.35	0.33	0.26	K	1	1.13	0.99
HD 95128	5882	4.38	0.04	0.06	0.03	0.04	0.04	2.80	KL	8	1.08	1.22
HD 99492	4954	4.77	0.36	0.32	0.22	0.37	0.35	1.36	K	1	0.88	0.76
HD 102117.....	5695	4.37	0.30	0.29	0.27	0.34	0.33	0.88	A	4	1.12	1.27
HD 106252	5869	4.36	−0.08	−0.07	−0.05	−0.07	−0.09	1.93	K	1	1.01	1.09
HD 108147	6156	4.29	0.09	0.10	0.04	0.00	0.06	6.10	A	3	1.19	1.22
HD 108874	5550	4.35	0.18	0.16	0.15	0.19	0.19	2.22	K	1	0.99	1.22
HD 114386.....	4819	4.71	0.00	0.06	−0.01	−0.07	0.03	0.59	K	1	0.75	0.76
HD 114729.....	5820	4.14	−0.26	−0.21	−0.08	−0.33	−0.30	2.29	K	1	0.99	1.46
HD 114762.....	5952	4.54	−0.65	−0.42	−0.36	−0.55	−0.69	1.77	L	4	0.90	1.22
HD 114783.....	5135	4.53	0.12	0.09	0.11	0.21	0.10	0.87	K	1	0.89	0.78
HD 117176.....	5544	4.07	−0.01	0.01	−0.02	−0.00	−0.04	2.68	L	3	1.11	1.86
HD 117207.....	5723	4.51	0.27	0.21	0.24	0.30	0.26	1.05	K	1	1.07	1.09
HD 117618.....	5963	4.35	0.00	0.03	0.02	0.02	0.00	3.19	A	2	1.08	1.19
HD 120136	6387	4.26	0.23	0.24	0.12	0.27	0.20	14.98	L	3	1.35	1.42

TABLE 1—*Continued*

Star ID	$T_{\rm eff}$ (K)	$\log g$ (cm s^{-2})	[Fe/H]	[Si/H]	[Ti/H]	[Na/H]	[Ni/H]	$v \sin i$ (km s^{-1})	Site	$N_{\rm obs}$	M_* ($M_\odot$)	R_* ($R_\odot$)
HD 128311.....	4965	4.83	0.20	0.27	0.07	0.08	0.17	3.65	K	1	0.84	0.73
HD 130322	5308	4.41	0.01	0.00	−0.11	−0.02	−0.04	1.61	K	1	0.89	0.83
HD 134987	5749	4.35	0.28	0.28	0.23	0.40	0.33	2.17	A	6	1.11	1.20
HD 136118.....	6097	4.05	−0.05	−0.05	−0.02	−0.11	−0.12	7.33	K	1	1.21	1.74
HD 137510	5965	3.99	0.37	0.35	0.30	0.50	0.41	7.98	K	1	1.36	1.97
HD 141937	5846	4.42	0.13	0.10	0.09	0.04	0.10	1.88	K	2	1.08	1.06
HD 142415	5901	4.38	0.09	0.08	0.04	0.01	0.04	3.43	A	3	1.09	1.03
HD 143761	5822	4.36	−0.20	−0.09	−0.06	−0.23	−0.21	1.56	KL	4	1.00	1.32
HD 145675	5387	4.52	0.46	0.42	0.40	0.62	0.49	1.56	K	1	1.00	0.94
HD 147513	5929	4.61	0.09	0.01	0.15	−0.12	0.01	1.55	K	1	1.07	0.93
HD 150706	5924	4.52	−0.00	0.11	−0.04	−0.19	−0.10	4.15	K	1	1.07	0.94
HD 154857	5605	3.99	−0.22	−0.19	−0.15	−0.24	−0.23	1.44	A	3	1.27	2.42
HD 160691	5784	4.30	0.29	0.28	0.26	0.40	0.34	3.12	A	3	1.16	1.31
HD 162020	4844	4.90	0.11	0.04	−0.01	−0.13	0.05	2.32	K	1	0.80	0.71
HD 168443	5579	4.25	0.08	0.10	0.12	0.07	0.08	2.20	K	1	1.05	1.56
HD 168746	5563	4.52	−0.08	0.03	0.08	−0.07	−0.07	0.00	K	1	0.92	1.12
HD 169830	6221	4.06	0.15	0.11	0.20	0.06	0.09	3.83	K	1	1.40	1.84
HD 177830	4948	4.03	0.55	0.40	0.34	0.59	0.61	2.54	K	1	1.48	2.99
HD 178911B.....	5667	4.55	0.28	0.26	0.26	0.34	0.30	1.94	K	4	1.07	1.14
HD 179949	6168	4.34	0.14	0.13	0.08	0.10	0.11	7.02	A	6	1.21	1.19
HD 183263	5936	4.40	0.30	0.27	0.28	0.33	0.33	1.56	K	1	1.18	1.21
HD 186427	5674	4.35	0.04	0.08	0.00	0.08	0.04	2.18	KL	7	0.99	1.15
HD 187123	5814	4.36	0.12	0.10	0.11	0.13	0.13	2.15	K	1	1.09	1.17
HD 188015	5745	4.44	0.29	0.27	0.25	0.42	0.33	0.00	K	1	1.09	1.10
HD 190228	5347	3.98	−0.18	−0.22	−0.12	−0.24	−0.23	1.85	K	1	1.21	2.40
HD 190360	5551	4.38	0.21	0.24	0.20	0.25	0.23	2.20	K	1	1.00	1.14
HD 192263	4975	4.60	0.05	0.07	−0.02	0.00	−0.02	2.63	K	1	0.81	0.75
HD 195019	5788	4.23	0.07	0.04	0.08	−0.03	0.03	2.47	K	1	1.06	1.38
HD 196050	5892	4.27	0.23	0.25	0.22	0.33	0.28	3.27	A	7	1.17	1.29
HD 196885	6185	4.23	0.20	0.20	0.17	0.18	0.18	7.75	K	1	1.27	1.35
HD 202206	5787	4.49	0.35	0.28	0.31	0.33	0.35	2.30	K	1	1.13	1.02
HD 208487	6067	4.34	0.02	0.04	0.03	−0.01	−0.01	4.61	A	4	1.13	1.15
HD 209458	6099	4.38	0.01	0.04	0.08	−0.04	−0.04	4.49	K	1	1.14	1.12
HD 210277	5555	4.49	0.21	0.22	0.22	0.24	0.21	1.80	K	1	1.01	1.05
HD 213240	5967	4.22	0.14	0.14	0.16	0.19	0.16	3.97	A	3	1.24	1.50
HD 216435	5999	4.15	0.24	0.22	0.24	0.28	0.27	5.78	A	5	1.30	1.72
HD 216437	5848	4.23	0.22	0.22	0.20	0.29	0.25	3.13	A	6	1.19	1.46
HD 216770	5368	4.44	0.21	0.47	0.13	0.42	0.27	1.04	K	1	1.02	1.00
HD 217014	5786	4.45	0.20	0.22	0.14	0.30	0.23	2.57	L	3	1.09	1.14
HD 217107	5704	4.54	0.39	0.35	0.32	0.43	0.39	0.00	K	1	1.09	1.08
HD 222582	5726	4.34	−0.03	0.00	−0.00	−0.01	−0.03	2.29	K	1	0.99	1.15

NOTE.—Table 1 is also available in machine-readable form in the electronic edition of the *Astrophysical Journal.*

In summary, we find that the occurrence of gas giant planets is a sensitive function of the metallicity of the host star, described by a power law in terms of the fraction of metal atoms. One-quarter of the FGK-type stars with [Fe/H] > 0.3 dex harbor Jupiter-like planets with orbital periods shorter than 4 yr. In contrast, gas giant planets are detected around fewer than 3% of the stars with subsolar metallicity. Significant increases in the percentage of stars with planets are likely to occur as the restricted planet parameter space is expanded to include planets with smaller velocity amplitudes or planets in wider orbits. Our estimate of the overall frequency of detectable planets may be biased slightly by the exclusion of certain rare classes of stars where stars cannot be detected with current techniques, e.g., chromospherically active stars or double-lined spectroscopic binaries. However, our methodology (measuring the metallicity of *all* stars in the sample) explicitly treats the significant metallicity bias in the planet search sample. This approach gives us a relatively unbiased measure of the dependence on metallicity for the vast majority of F, G, and K-type stars. In contrast, using the metallicity distribution of stars in a volume-limited sample as a proxy for metallicity in the planet search sample would introduce significant bias.

3.1. *The Metal-poor Stars*

The two metallicity bins with [Fe/H] less than -0.5 dex contain very few stars. The bin with $-1.0 <$ [Fe/H] < -0.75 contains only four stars, and the $-0.75 <$ [Fe/H] < -0.5 bin contains 25 stars. In addition, there are 13 stars with [Fe/H] < -1.0 in the subset of 850 well-observed stars. No planets have been detected among these stars, so the error bars were assigned by assuming that the planet occurrence rate was the same as that in the $-0.5 <$ [Fe/H] < -0.25 bin (i.e., 3.8%). The error bar for the lowest metallicity bin is then $3.8/(7 \times 3.8)$, or 14.3%, because of the very small number of observed stars. The error bar in the next metallicity bin is $3.8/(28 \times 3.8)$, or 3.6%. While the small number of stars with [Fe/H] < -0.5 does not offer a strong constraint on the occurrence rate of planets orbiting these stars, we note that the Geneva team has guaranteed HARPS time to study

TABLE 2

ORBITAL PARAMETERS FOR EXTRASOLAR PLANETS

Star ID	N_{pl}	Period (days)	K (m s^{-1})	Eccentricity	$M \sin i$ (M_J)	a_{rel} (AU)	Publication Year
BD −10 3166	1	3.49	59.89	0.07	0.44	0.04	2000
HD 142	1	331.87	31.59	0.37	1.16	1.01	2001
HD 1237	1	133.80	164.00	0.51	3.47	0.51	2000
HD 2039	1	1192.58	127.82	0.68	5.46	2.33	2002
HD 3651	1	62.23	15.90	0.63	0.22	0.30	2002
HD 4203	1	400.94	49.29	0.46	1.75	1.12	2001
HD 4208	1	812.20	18.22	0.05	0.76	1.62	2001
HD 8574	1	228.18	64.00	0.31	2.01	0.77	2001
HD 9826	3	4.62	70.20	0.01	0.69	0.06	1996
HD 9826	3	241.50	53.90	0.28	1.90	0.83	1999
HD 9826	3	1284.00	61.10	0.27	3.78	2.53	1999
HD 10647	1	1040.00	18.00	0.18	0.94	2.07	2004
HD 10697	1	1077.91	114.19	0.11	6.29	2.16	1999
HD 12661	2	263.00	75.00	0.33	2.38	0.83	2000
HD 12661	2	1530.00	27.00	0.20	1.60	2.68	2002
HD 13445	1	15.77	375.88	0.04	3.87	0.11	1998
HD 16141	1	75.56	11.25	0.21	0.25	0.37	2000
HD 17051	1	311.29	58.82	0.24	2.11	0.95	1999
HD 20367	1	469.50	29.00	0.32	1.11	1.22	2002
HD 22049	1	2675.00	13.70	0.28	0.79	3.54	2003
HD 23079	1	738.46	55.28	0.10	2.47	1.61	2001
HD 23596	1	1548.00	126.00	0.30	7.83	2.80	2002
HD 27442	1	423.84	30.71	0.07	1.48	1.26	2001
HD 28185	1	383.00	161.00	0.07	6.63	1.11	2001
HD 30177	1	2819.65	142.18	0.30	9.85	3.99	2002
HD 33636	1	2447.29	164.52	0.53	9.37	3.58	2001
HD 34445	1	126.00	24.00	0.40	0.58	0.51	2004
HD 37124	2	154.60	37.80	0.09	0.87	0.53	1999
HD 37124	2	31.00	19.60	0.34	0.25	0.18	2004
HD 38529	2	2207.40	169.10	0.33	13.10	3.76	2002
HD 38529	2	14.31	54.70	0.28	0.80	0.13	2000
HD 39091	1	2063.82	196.92	0.62	10.31	3.28	2001
HD 40979	1	267.20	108.00	0.23	3.74	0.86	2002
HD 45350	1	890.00	33.00	0.78	1.03	1.86	2004
HD 46375	1	3.02	34.50	0.04	0.23	0.04	2000
HD 49674	1	4.95	13.14	0.17	0.11	0.06	2002
HD 50499	1	2990.00	23.30	0.32	1.84	4.40	2004
HD 50554	1	1249.59	81.87	0.50	3.87	2.30	2001
HD 52265	1	119.10	38.75	0.19	1.04	0.50	2000
HD 68988	1	6.28	189.74	0.15	1.90	0.07	2001
HD 70642	1	2231.00	32.00	0.10	2.11	3.39	2003
HD 72659	1	3537.15	42.31	0.26	3.26	4.69	2002
HD 73256	1	2.55	267.00	0.04	2.07	0.04	2002
HD 73526	1	184.11	114.76	0.44	3.03	0.65	2002
HD 74156	2	2650.00	125.00	0.35	9.28	4.05	2001
HD 74156	2	51.52	112.00	0.65	1.82	0.29	2001
HD 75289	1	3.51	53.52	0.01	0.46	0.05	1998
HD 75232	4	2.81	6.66	0.17	0.05	0.05	2004
HD 75732	4	44.28	13.00	0.34	0.20	0.24	2002
HD 75732	4	14.65	72.20	0.02	0.82	0.11	1996
HD 75732	4	5360.00	49.30	0.16	3.95	5.82	2002
HD 76700	1	3.97	25.05	0.13	0.21	0.05	2002
HD 80606	1	111.81	411.00	0.93	3.79	0.46	2001
HD 82943	2	444.60	46.00	0.41	1.76	1.20	2000
HD 82943	2	221.60	34.00	0.54	0.95	0.76	2001
HD 83443	1	2.98	58.05	0.05	0.41	0.04	2000
HD 88133	1	3.41	26.00	0.00	0.22	0.05	2004
HD 89307	1	3090.00	39.70	0.27	2.73	4.15	2004
HD 89744	1	256.61	275.26	0.67	8.60	0.92	2000
HD 92788	1	327.39	98.62	0.33	3.43	0.97	2000
HD 95128	2	1089.00	49.30	0.06	2.62	2.13	1996
HD 95128	2	2594.00	11.10	0.10	0.79	3.79	2001

TABLE 2—*Continued*

Star ID	N_{pl}	Period (days)	K (m s^{-1})	Eccentricity	$M \sin i$ (M_J)	a_{rel} (AU)	Publication Year
HD 99492	1	17.00	10.40	0.05	0.12	0.12	2004
HD 102117	1	20.80	12.90	0.05	0.19	0.15	2004
HD 106252	1	1503.61	150.45	0.57	7.03	2.58	2001
HD 108147	1	10.89	27.30	0.40	0.31	0.10	2003
HD 108874	2	397.43	49.58	0.14	1.77	1.06	2002
HD 108874	2	1724.00	18.80	0.42	1.00	2.81	2004
HD 114386	1	872.00	27.00	0.28	1.01	1.62	2002
HD 114729	1	1131.48	17.64	0.31	0.85	2.12	2002
HD 114762	1	83.89	616.66	0.34	11.60	0.36	1988
HD 114783	1	494.67	28.51	0.09	1.02	1.18	2001
HD 117176	1	116.69	315.22	0.40	7.44	0.48	1996
HD 117207	1	2617.05	30.00	0.16	2.11	3.81	2004
HD 117618	1	52.00	11.80	0.25	0.22	0.28	2004
HD 120136	1	3.31	471.35	0.01	4.22	0.05	1996
HD 128311	1	420.51	84.89	0.30	2.65	1.04	2002
HD 128311	2	919.00	79.80	0.29	3.24	1.74	2004
HD 130322	1	10.72	115.00	0.04	1.15	0.09	1999
HD 134987	1	258.50	49.35	0.25	1.61	0.82	1999
HD 136118	1	1208.72	212.87	0.36	11.81	2.37	2002
HD 137510	1	778.00	497.00	0.37	25.63	1.83	2004
HD 141937	1	653.22	234.50	0.41	9.59	1.51	2001
HD 142415	1	388.00	52.00	0.50	1.71	1.07	2004
HD 143761	1	39.85	64.24	0.04	1.08	0.23	1997
HD 145675	1	1773.08	88.75	0.38	4.89	2.87	1999
HD 147513	1	540.40	31.00	0.52	1.11	1.33	2002
HD 150706	1	264.90	33.00	0.38	1.01	0.83	2002
HD 154857	1	398.50	52.00	0.51	1.90	1.15	2004
HD 160691	3	9.50	4.10	0.00	0.04	0.09	2004
HD 160691	3	664.19	42.76	0.26	1.95	1.56	2001
HD 160691	3	2986.00	51.00	0.57	3.27	4.26	2004
HD 162020	1	8.43	1813.00	0.28	15.04	0.08	2000
HD 168443	2	1770.00	289.00	0.20	17.38	2.91	2001
HD 168443	2	58.10	472.70	0.53	7.88	0.30	1999
HD 168746	1	6.40	27.00	0.08	0.23	0.07	2000
HD 169830	1	229.90	83.00	0.35	2.94	0.82	2000
HD 169830	1	1487.00	36.00	0.00	2.53	2.85	2004
HD 177830	1	408.38	37.69	0.10	1.78	1.23	1999
HD 178911B	1	71.50	343.00	0.14	7.27	0.35	2001
HD 179949	1	3.09	117.96	0.00	0.96	0.04	2001
HD 183263	1	631.45	86.00	0.37	3.77	1.52	2004
HD 186427	1	798.94	51.24	0.67	1.73	1.68	1996
HD 187123	2	2750.00	27.00	0.50	1.70	3.95	2004
HD 187123	1	3.10	67.96	0.02	0.52	0.04	1998
HD 188015	1	470.85	42.00	0.26	1.64	1.22	2004
HD 190228	1	1121.00	90.00	0.50	4.53	2.25	2000
HD 190360	1	2613.00	17.50	0.00	1.19	3.72	2002
HD 192263	1	24.33	50.50	0.03	0.63	0.15	2003
HD 195019	1	18.20	271.38	0.02	3.65	0.14	1998
HD 196050	1	1316.24	48.51	0.21	2.83	2.47	2002
HD 196885	1	386.00	46.00	0.30	1.84	1.12	2004
HD 202206	1	256.00	564.80	0.43	17.33	0.82	2000
HD 208487	1	129.10	17.00	0.35	0.43	0.52	2004
HD 209458	1	3.53	86.52	0.11	0.70	0.05	1999
HD 210277	1	434.29	39.46	0.46	1.31	1.12	1999
HD 213240	1	951.00	91.00	0.45	4.53	2.03	2001
HD 216435	1	1442.92	24.54	0.34	1.53	2.73	2000
HD 216437	1	1331.70	37.46	0.36	2.13	2.51	2002
HD 216770	1	118.00	33.00	0.32	0.76	0.47	2004
HD 217014	1	4.23	54.99	0.01	0.46	0.05	1995
HD 217107	1	7.13	140.23	0.14	1.40	0.07	1998
HD 217107	2	2500.00	55.00	0.53	3.31	3.71	2004
HD 222582	1	572.00	191.26	0.76	5.03	1.34	1999

NOTE.—Table 2 is also available in machine-readable form in the electronic edition of the *Astrophysical Journal.*

TABLE 3
STARS WITH UNIFORM PLANET DETECTABILITY

Star ID	Planet/Star
HD 142	P
HD 2039	P
HD 4203	P
HD 8574	P
HD 10697	P

NOTE.—Table 3 is published in its entirety in the electronic edition of the *Astrophysical Journal*. A portion is shown here for guidance regarding its form and content.

more than 100 metal-poor stars (Mayor et al. 2003). In addition, a Doppler survey of ~150 low-metallicity stars has been underway at Keck for the past two years (Sozzetti et al. 2004). No planets have been announced from either of these surveys, suggesting that the rate of occurrence of Jovian-mass planets with orbital periods less than 3 yr does not exceed (and is likely lower than) a few percent around metal-poor stars.

A single substellar object, HD 114762b, with $M \sin i \sim 11 M_J$ has been found orbiting a metal-poor ([Fe/H] = −0.655) field star (Latham et al. 1989). Interestingly, we measure a low $v \sin i$ (1.7 km s^{-1}) for this F-type star. Fewer than 5% of the stars with comparable spectral type have $v \sin i < 2.0$ km s^{-1}, suggesting that this particular star may be viewed close to pole-on. Assuming that the stellar rotation axis is aligned with the orbital rotation axis, it is possible that the companion to HD 114762 may have a substantially higher mass, conceivably even a stellar mass, a suggestion first made by Cochran et al. (1991).

It has been suggested that the paucity of spectral lines in metal-poor stars results in poorer detectability that impedes the detection of Jovian-mass planets. To address this issue, we calculated the mean radial velocity error for stars in each 0.25 dex metallicity bin. For [Fe/H] between −0.75 and 0.5, the mean Doppler precision is 4 m s^{-1}. The lowest metallicity bin only suffers a modest degradation in velocity precision to ~6 m s^{-1}. Thus, there is no significant detectability bias against the detection of planets in the parameter space that we have defined to have uniform detectability. If gas giant planets orbit metal-poor stars as often as they orbit solar-metallicity stars, it seems very likely that they would have been detected by now.

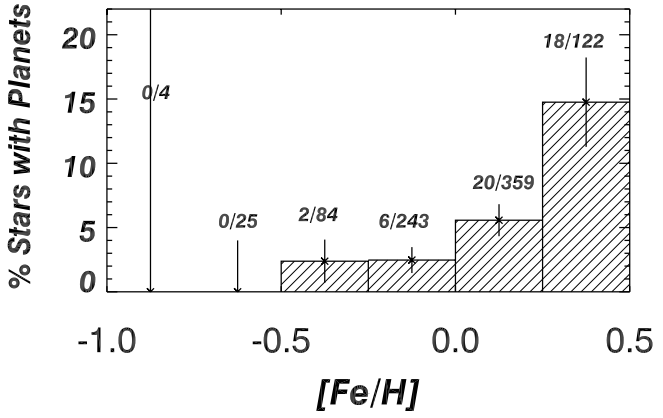

FIG. 4.—Percentage of stars with detected planets rises with iron abundance. In all, a subset of 850 stars were grouped according to metallicity. This subset of stars had at least 10 Doppler measurements over 4 yr, providing uniform detectability for the presence of planets with velocity amplitudes greater than 30 m s^{-1} and orbital periods less than 4 yr. The numbers above each bar on the histogram indicate the ratio of planets to stars in each bin. Thirteen stars had [Fe/H] < −1.0, and no planets have been discovered around these stars.

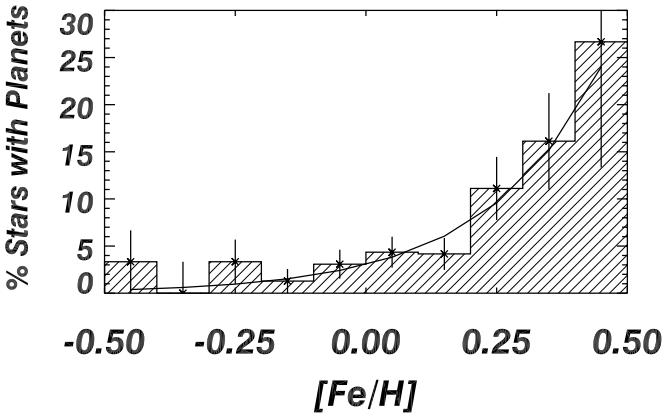

FIG. 5.—Same results as Fig. 4, but divided into 0.1 dex metallicity bins. The increasing trend in the fraction of stars with planets as a function of metallicity is well fitted with a power law, yielding the probability that an FGK-type star has a gas giant planet: $\mathcal{P}(\text{planet}) = 0.03[(N_{Fe}/N_H)/(N_{Fe}/N_H)_\odot]^{2.0}$.

3.2. *The Volume-limited Sample*

A volume-limited sample is often desirable as an unbiased sample, and virtually all spectroscopic investigations of the planet-metallicity correlation have referenced such a sample as a control. We contend that a volume-limited sample is not the best comparison sample for this investigation because it does not necessarily represent the stars on Doppler surveys. To investigate this, we defined a volume-limited subset of 230 FGK-type stars analyzed with SME. Figure 6 shows the density of the entire (1040 star) planet search sample as a function of distance for specified ranges of absolute visual magnitude. The points on each curve mark the distance where the sample size increments by about 40 stars. Intrinsically faint stars dominate the 20 pc sample, and the sample composition gradually shifts to earlier type, intrinsically bright stars at larger distances. We define the volume-limited sample to have a radius of 18 pc, inside of which the number of FGK-type stars per unit volume on the planet search programs is nearly constant as a function of distance. Beyond this distance the number density of intrinsically faint stars begins to decline rapidly.

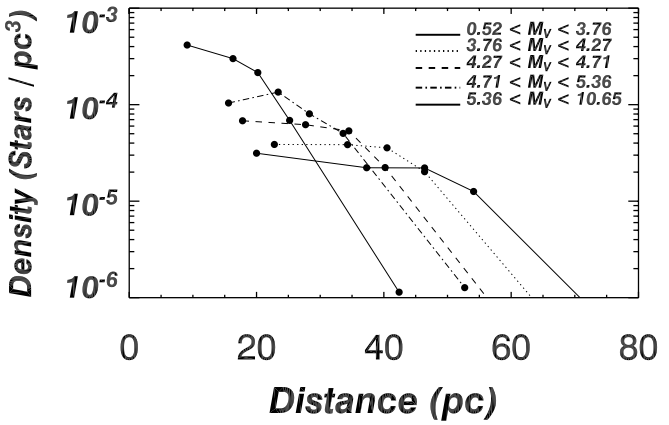

FIG. 6.—Stellar density for a range of absolute visual magnitudes calculated in distance bins, each with 41–43 stars. Intrinsically faint stars dominate the nearby solar neighborhood but are rapidly lost beyond 20 pc. Intrinsically bright stars become the dominant constituent of the planet search samples at distances greater than about 40 pc.

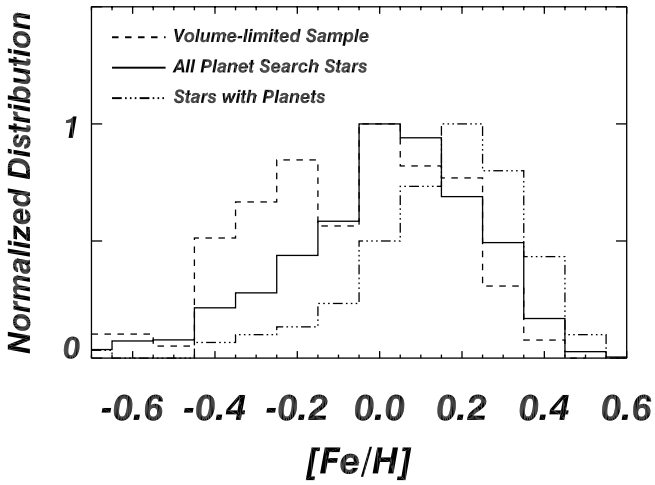

FIG. 7.—18 pc volume-limited sample extracted from the SME-analyzed stars and compared with the overall sample of planet search stars and the subset of stars known to have extrasolar planets. The distributions are represented according to the legend in the figure. All distributions have been normalized to unity to aid comparison. A K-S test shows that the volume-limited sample of stars has a distribution that is metal-poor by almost 0.1 dex relative to the overall planet search sample and stars with planets have a distribution that is more metal-rich than the entire sample by 0.13 dex. The metallicity distribution of stars with planets is 0.23 dex more metal-rich than the volume-limited sample.

Figure 7 compares the metallicity distribution for three samples: (1) the volume-limited sample, (2) all analyzed stars on the planet search programs, and (3) the subset of analyzed stars with detected planets. To aid comparison, all distributions have been normalized to a peak value of unity. It is clear that these three samples have different metallicity distributions. The overall sample of planet search stars is more metal-rich than the volume-limited sample, and the set of stars with planets is more metal-rich than the other two samples. The offset of the distributions was calculated by applying an incremental shift of 0.003 dex and using a double-sided Kolmogorov-Smirnov (K-S) test to assess the probability that any two samples were drawn from the same parent population. The K-S probabilities show that stars on the planet search programs have a metallicity distribution that is shifted by 0.09 dex relative to the volume-limited sample. An explanation for this offset, discussed below, is that the overall sample contains more high-mass, metal-rich stars than the volume-limited sample. Thus, stars with planets are indeed drawn from a parent sample that is somewhat more metal-rich than a volume-limited sample, emphasizing the importance of referencing any metallicity comparisons to the parent Doppler sample. The stars with planets are metal-rich by +0.13 dex relative to the overall planet search sample, but in comparison, stars with planets are 0.226 dex more metal-rich than the volume-limited sample.

4. METALLICITY AS A FUNCTION OF CZ DEPTH

The data were examined for correlations between metallicity and CZ depth in the main-sequence stars. In Figure 8, the stellar metallicity, [M/H], is plotted as a function of $T_{\rm eff}$ for all analyzed main-sequence stars. A first-order polynomial fit to the data has a slope consistent with zero, indicating that no correlations exist between [M/H] and $T_{\rm eff}$. We emphasize that no corrections have been made to [M/H] that would affect or remove a linear trend if one existed. The second key feature of this [M/H] distribution is the behavior of the upper boundary of the metallicity distribution. If the upper boundary was increasing with $T_{\rm eff}$ (or equivalently, with decreasing CZ depth), this would support an accretion hypothesis for metallicity enrichment. However, no rise in the upper boundary of the metallicity distribution is observed.

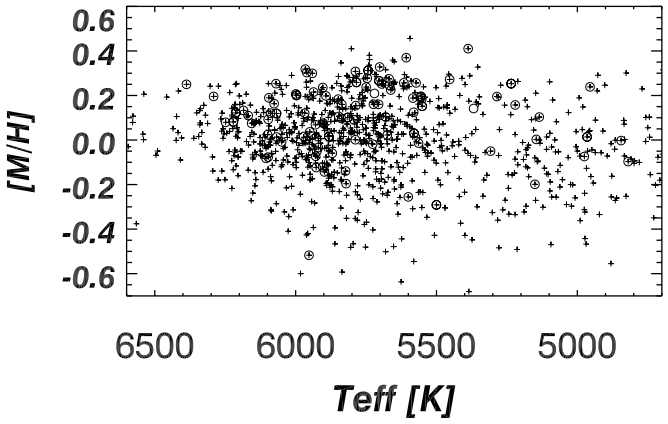

FIG. 8.—Stellar metallicity, [M/H], as a function of $T_{\rm eff}$. A linear fit to the data has zero slope. No trend in metallicity is seen with $T_{\rm eff}$ or long the top edge of the metallicity boundary.

As described in § 2.1, stellar masses were derived from interpolation of Y^2 isochrones and have an expected relative accuracy of ~10%. Figure 9 shows a fairly obvious correlation between stellar mass and metallicity. Since a correlation between metallicity and the occurrence of planets has been clearly quantified (Fig. 5), the correlation between stellar mass and metallicity implies that there should also be a (spurious) correlation between stellar mass and the occurrence of planets.

We again make use of the set of 850 stars for which Doppler observations provide uniform sensitivity to planets with $K > 30$ m s^{-1} and orbital periods shorter than 4 yr. This time, the stars are binned by stellar mass and the fraction of stars with extrasolar planets is calculated for each mass bin. Figure 10 shows that the occurrence of planets increases linearly with stellar mass. This result begs the question: Which parameter (stellar mass or metallicity) is fundamentally correlated with the occurrence of gas giant planets? If a primordial metallicity threshold is responsible for the planet-metallicity correlation, then we expect that the same offset in the metallicity distribution will be observed at all

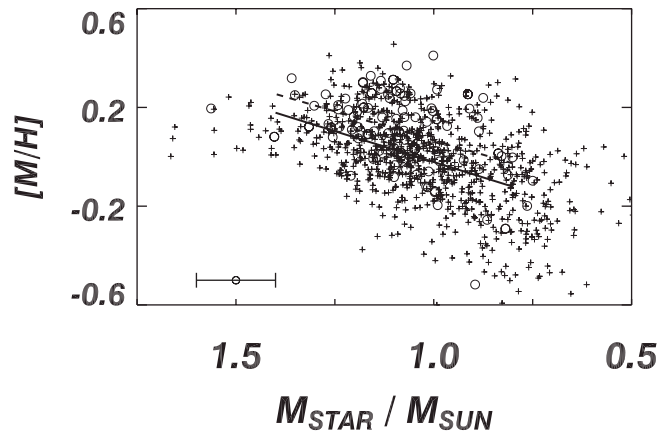

FIG. 9.—Linear correlation found between stellar mass and metallicity. Stellar masses were derived by interpolating over a grid of Yale stellar evolution tracks. A fit to the data (solid line for all stars and dashed line for stars with planets) shows a trend that is likely a result of stellar evolution, which removes high-mass, low-metallicity stars as candidates for the planet search programs. In addition, higher mass, metal-rich stars will be red enough to meet the $B - V$ selection criterion.

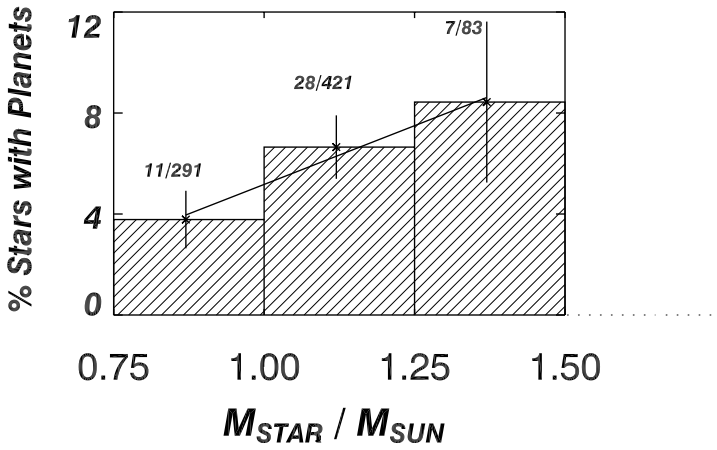

FIG. 10.—Set of 850 stars with uniform detectability ($K > 30$ m s^{-1} and periods shorter than 4 yr) binned according to stellar mass and the fraction of stars with detected gas giant planets calculated for each bin. Only well-populated bins with planet detections are shown here. At first glance, the planet occurrence rate appears to be correlated with stellar mass. However, the underlying reason correlation is likely a stellar mass-metallicity correlation.

stellar masses. However, if higher stellar mass enhances planet formation independent of metallicity, perhaps by virtue of higher surface density primordial disks, then higher mass stars could start forming planets at lower metallicities and we would expect a smaller offset in the metallicity distribution between stars with and without planets.

The data in Figure 9 are consistent with the former scenario, suggesting that metallicity is probably the primary agent in the planet correlation. A linear fit between stellar mass and [M/H] was determined for stars with and without detected planets and overplotted on Figure 9. Importantly, both fits have the same slope: 0.8 $M_\odot$ stars *with* planets have a metallicity distribution that is shifted by +0.12 dex with respect to 0.8 $M_\odot$ stars *without* planets, and 1.2 $M_\odot$ stars *with* planets have a metallicity distribution that is shifted by +0.12 dex with respect to 1.2 $M_\odot$ stars *without* planets. Independent of stellar mass, stars with planets have a metallicity distribution shifted by 0.12 dex relative to stars without planets. Thus, there is no evidence that stellar mass significantly enhances the formation probability of gas giant planets.

So, what does the correlation between stellar mass and metallicity mean? It seems likely that this trend is a consequence of stellar evolution and the $B - V > 0.4$ selection criteria imposed by the planet search programs. At the age of the Galaxy, most stars of subsolar mass are still unevolved, main-sequence stars. The distribution of these low-mass stars probably represents a relatively unbiased range of masses, metallicities, and ages. However, the situation is different for stars more massive than the Sun. At the turnoff mass of the Galaxy, the metal-poor late F and early G type stars evolve away from the main sequence sooner than the higher metallicity stars and there are simply fewer of these stars to select for a magnitude-limited sample. In addition, while metal-poor stars are still forming today, they are not being formed at the same rate that they are evolving away. Finally, the number of high-mass, high-metallicity stars is enhanced because these stars are intrinsically redder and they cross the $B - V$ sample selection boundary.

The correlation between stellar mass and metallicity likely explains the fact that the overall planet search sample is more metal-rich than the volume-limited subset (§ 3.2). The volume-limited sample is populated with more low-mass stars than the overall planet search sample simply because the latter sample is magnitude-limited. Therefore, the planet search sample contains more high-mass stars. As discussed above, this effectively builds in an offset toward a higher metallicity distribution.

4.1. *Subgiants*

At the present time, stellar metallicity appears to be the strongest predictor for the presence of gas giant planets. However, it would be useful to survey a wider range of stellar masses in order to better assess planet occurrence as a function of stellar mass. The number of stars on Doppler surveys declines for stellar masses greater than 1.2 $M_\odot$ because it becomes increasingly difficult to obtain high velocity precision for stars earlier in spectral type than F7. As the effective temperature of stars increases, the number of spectral lines available for cross-correlation to determine radial velocity decreases. In addition, early-type stars rotate faster and as a consequence have broader lines than later type stars. Broad spectral lines do not centroid as precisely in a cross-correlation measurement, so velocity precision declines with increasing $v \sin i$.

The best way to carry out a Doppler survey of more massive stars is to observe a sample of subgiants. On the subgiant branch, evolved stars whose progenitors were earlier F-type stars have cooled and spun down. The Doppler precision that can be achieved with subgiants is typically $\sim$5–7 m s^{-1}, making it straightforward to detect gas giant planets around somewhat more massive stars.

About 60 subgiants were added to the Lick planet search program in 2002, and an additional set of 200 subgiants has recently been added to the Lick program (J. Johnson 2004, private communication). The goal of the subgiant survey is twofold: to learn about planet occurrence around high-mass stars and to compare the metallicity distributions of main-sequence and subgiant planet-bearing stars. A fit to $T_{\rm eff}$ and M_V was used to define the lower edge of the main sequence, and stars that were more than 1.5 mag above the main sequence were designated as subgiants. Figure 11 shows the H-R diagram for SME-analyzed stars and identifies the stars flagged as subgiants. The circled subgiants have detected extrasolar planets. Currently, there are 86 well-observed subgiants on the planet search programs, and nine of these subgiants have detected planets. Thus, extrasolar planets are detected around subgiants as often as around main-sequence stars.

As previously noted, there are two favored explanations for high metallicity in stars with planets: (1) they were born from

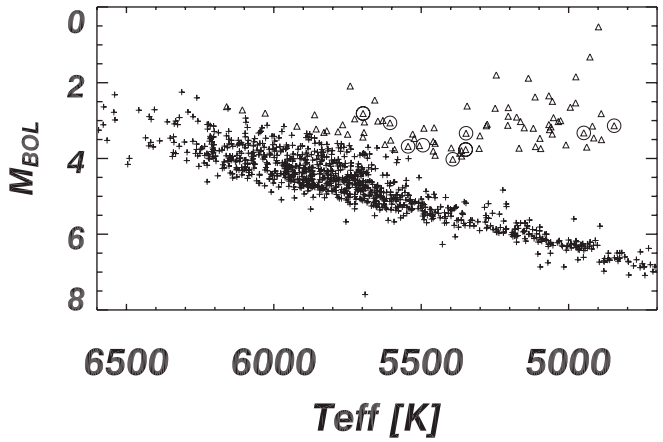

FIG. 11.—Stars with $M_{\rm bol} > 1.5$ mag above the lower boundary of the main sequence are identified as subgiants (*open triangles*). Subgiants with detected planets are circled. Main-sequence stars are represented with plus signs.

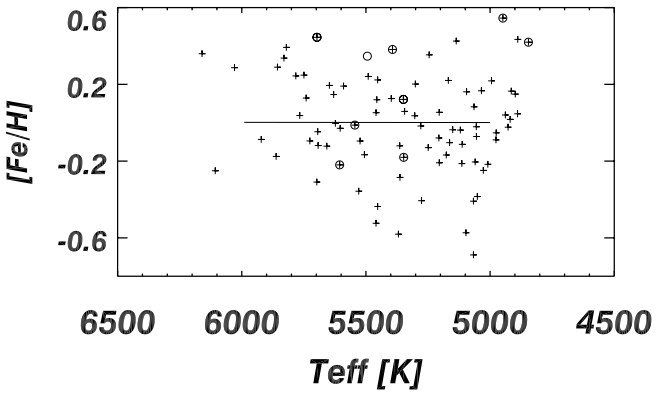

FIG. 12.—Stars should experience increasing dilution of their CZs as they evolve across the subgiant branch; however, no metallicity gradient is observed along the subgiant branch.

molecular clouds with high metallicity or (2) the metal content of the CZ was elevated by late-stage accretion of gas-depleted material. In the first case, the star would be metal-rich throughout, and in the second case, the CZ would have higher metallicity than the underlying radiative core. The subgiants are of key importance because as they evolve, the outer convective envelope is diluted by material in the stellar interior. If the high metallicity that is correlated with the presence of Jovian planets is limited to the convective envelope of main-sequence stars, then subgiants with planets should show systematically lower metallicity.

Furthermore, as the degree of CZ dilution increases redward along the subgiant branch, a metallicity gradient might be expected as a function of $T_{\rm eff}$. The measured [Fe/H] for stars along the subgiant branch is plotted in Figure 12 (*bottom*). The subgiants show scatter in their metallicities typical of main-sequence stars; however, a linear fit to metallicity as a function of $T_{\rm eff}$ is flat. No metallicity gradient is observed along the subgiant branch.

In addition, there is no evidence for lower metallicity in the subgiant stars. The median metallicity of subgiants without detected planets is -0.01 dex, while the median metallicity of subgiants with planets is 0.35 dex. A K-S test shows that the metallicity distribution of subgiants with planets is consistent with that of main-sequence stars with planets, and both subgiants and main-sequence stars with planets are more metal-rich than their counterparts without detected planets. Therefore, subgiants do not exhibit any evidence for dilution. These data strongly support the hypothesis that stars with planets are metal-rich throughout their interiors and that Jovian planet formation is enhanced by high metallicity in the primordial disk.

4.2. *Elements with Different Condensation Temperatures*

In addition to deriving a global metallicity, [M/H], abundances for Fe, Na, Ni, Si, and Ti are individually set as free parameters to search for trends in element abundances as a function of condensation temperature. Initially, abundances of highly volatile elements, carbon and oxygen, were also included as free parameters. However, in the final spectroscopic analysis, only those elements with demonstrated reliable results were allowed to float. For the individual chemical elements that we analyzed, Lodders (2003) calculates self-consistent equilibrium condensation temperatures in a solar system composition gas for Na (958 K), Fe (1334 K), Ni (1353 K), Si (1529 K), and Ti (1582 K). As Gonzalez (1997) pointed out, if refractory elements (defined as elements with condensation temperatures near or above the condensation temperature of iron) were more abundant than volatile elements (defined on the basis of low condensation temperatures relative to iron), then this might signal late-stage accretion as a mechanism for elevating stellar metallicities.

The abundance ratios as a function of [Fe/H] for the analyzed set of individual elements are plotted in Figure 13. As discussed in VF05, the individual abundances have applied corrections so that no trends remain relative to global metallicity as a function of effective temperature. The prominent trends observed in Figure 13 appear to be real. However, the meaningful comparison to be made is a relative one between stars with and without detected planets. No differences are observed between stars with planets and stars without planets over the studied range of condensation temperatures. Apparently, stars harboring planets have abundances of refractory elements that are no different from those of stars without planets. This suggests that accretion of dust and planetesimals by the star plays little role in the observed chemical abundances.

5. OTHER METALLICITY TRENDS

5.1. *Multiplanet Systems*

The number of stars with multiple-planet systems continues to grow each year. In the most statistically complete Doppler survey of $\sim$100 stars observed since 1989 at Lick Observatory, half of the stars with one detected planet also have additional planets. There are now 14 known multiplanet systems. Although this is in the realm of small number statistics, it is notable that among the 22 planet-bearing stars with subsolar metallicity only 1 star (4.5%) has a double planet system. In contrast, 13 of 98 (13%) stars with greater than solar metallicity have multiple-planet systems. Although this trend is somewhat suggestive, it is not yet statistically significant. The mean metallicity of stars with multiplanet systems is [Fe/H] = 0.18, with an uncertainty in the mean of 0.05, while the mean metallicity of stars where only one planet has been detected is [Fe/H] = 0.14, with an uncertainty in the mean of 0.02. It will be interesting to see whether this trend continues as more multiplanet systems are detected.

5.2. *Total Planet Mass*

Although many undetected lower mass planets may exist in systems with known gas giant planets, the detected planets probably account for the bulk of planetary mass in the inner few AU of the host stars. Since the occurrence of planets is a sensitive function of stellar metallicity, it is possible that the amount of the protoplanetary disk mass that is ultimately locked up as planets is also correlated with metallicity.

In Figure 14, the planet mass ($M \sin i$) is plotted as a function of stellar metallicity. All stars with known planets that were analyzed with SME are included in this figure. In the case of multiple-planet systems, the individual planet masses are totaled and are represented in Figure 14 with filled circles. The two largest filled circles represent the triple planet system around υ And and the quadruple planet system around 55 Cnc. Single planets are represented with plus signs. The mass of detected planets rises with increasing metallicity, suggesting that the total amount of disk material ultimately locked up in the form of planets may be regulated by stellar metallicity. Again, the number of gas giant planets around metal-poor stars is very small, so while suggestive, this is not an overly compelling trend.

5.3. *Orbital Parameters*

The orbits of detected extrasolar planets reveal dramatic differences from planets in our solar system. Solar system planets reside in nearly circular orbits, while the Doppler-detected

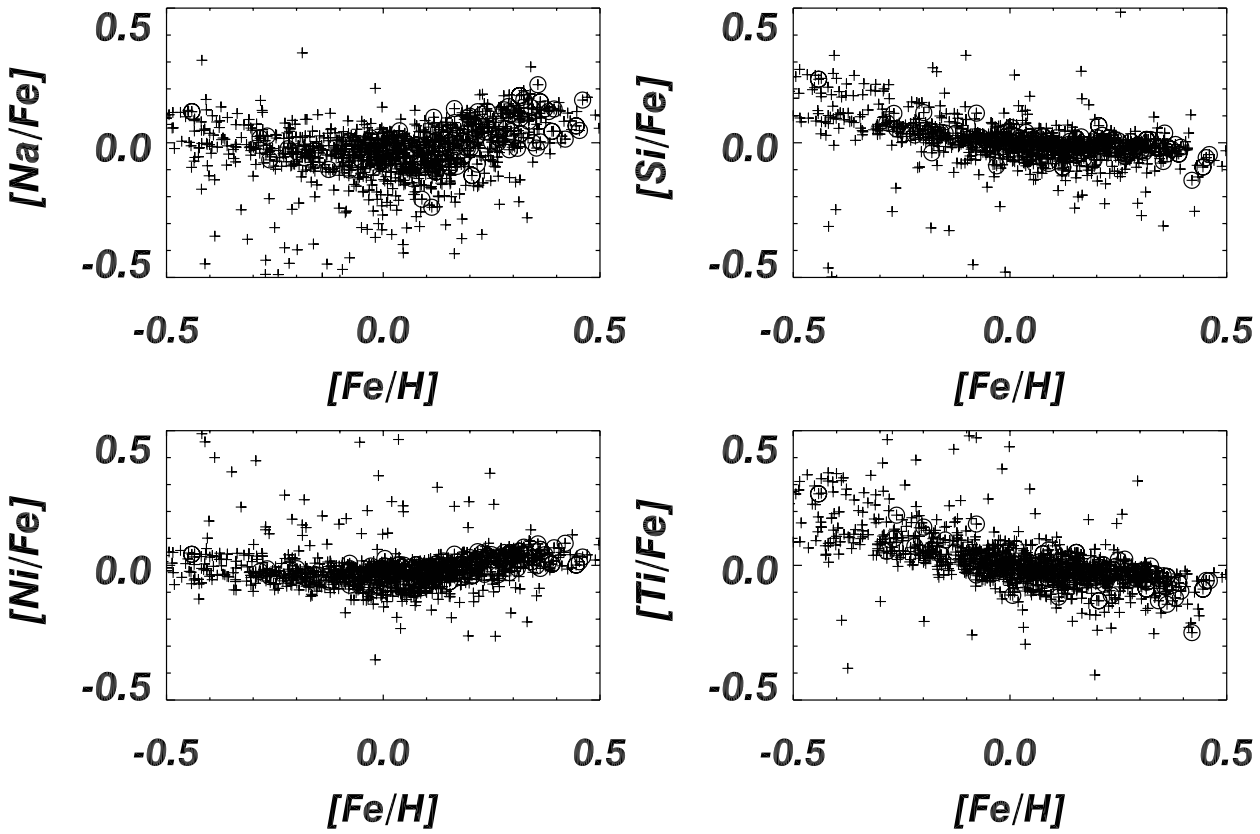

FIG. 13.—Abundance ratios of Na, Si, Ni, and Ti relative to Fe and as a function of [Fe/H]. Plus signs represent the analyzed stars, and stars with planets are circled. No differences are observed in abundance distributions for stars with and without planets.

planets exhibit eccentricities that range between nearly circular and highly eccentric. One unusual system, HD 80606, has a record-breaking eccentricity of 0.94. Another striking difference is that many extrasolar gas giant planets have orbital periods of days, placing them within 0.1 AU of their host star. We consider whether the high metallicity that is correlated with the very existence of extrasolar planets could also influence the final orbital architecture of the planets.

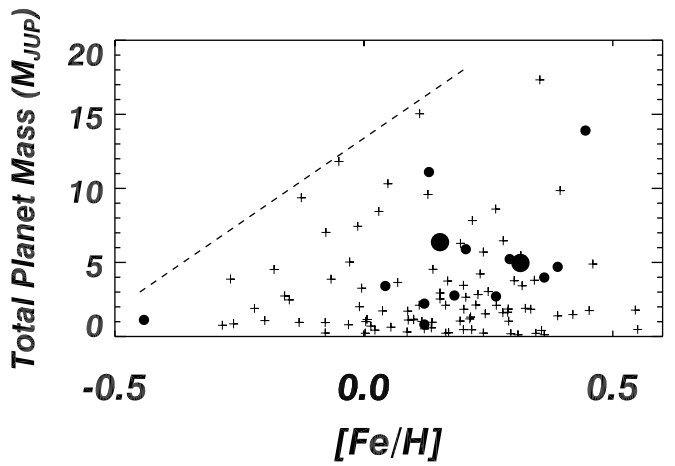

FIG. 14.—Planet mass ($M \sin i$) plotted for all detected planets as a function of metallicity. Plus signs represent single planets, and filled circles represent the total mass for multiple-planet systems. There is a suggestion that the maximum total planet mass may rise with increasing stellar metallicity, as indicated by the overplotted line.

The orbital parameters for the known extrasolar planets are tabulated in Table 2. As a first step, the stars were grouped according to the orbital periods of the detected planets, and the distribution of stellar and orbital parameters is summarized in Table 4, with the standard deviation from the mean listed in parentheses. The longest orbital period range (1000 days $< P <$ 10,000 days) does not span a full logarithmic bin because the maximum observed orbital periods are effectively terminated at 4000 days by the time baseline of the Doppler surveys.

Our motivation for grouping the stars by orbital period is to compare planetary systems that may have experienced different degrees of orbital migration, since migration and late-stage accretion could be physically linked. The naive underlying assumption is that close-in planets have experienced significant inward migration with a stronger accompanying accretion while planets in wide orbits have experienced less migration and therefore have less (late-stage) accretion. Cases in which planets in wide orbits are accompanied by additional interior planets are omitted from Table 4 because the inner planets in these systems may have played an additional role in the accretion history of the star.

Udry et al. (2003) note the existence of a "period valley" with an absence of exoplanets with masses larger than $2M_J$ in the period range from 10 to 100 days. It is interesting that the host stars of planets with orbital periods in this range have systematically lower metallicity than stars in the adjacent period bins. By virtue of this lower metallicity, these stars are expected to have fewer and lower mass planets. It is certainly possible that small number statistics are at play here. It would be very helpful to identify several additional short-period planets to better understand the observed period valley.

TABLE 4
Distribution of Orbital Parameters

Orbital Period (days)	$\langle T_{\rm eff} \rangle$ (K)	$\langle$[Fe/H]$\rangle$	$\langle$ecc$\rangle$	$\langle M_* \rangle$ ($M_\odot$)	$\langle R_* \rangle$ ($R_\odot$)	$N_{\rm stars}$
1–10	5730 (90)	0.23 (0.03)	0.07 (0.02)	1.11 (0.03)	1.21 (0.07)	18
10–100	5555 (80)	0.07 (0.06)	0.23 (0.05)	1.02 (0.04)	1.24 (0.10)	20
100–1000	5737 (57)	0.16 (0.03)	0.37 (0.03)	1.13 (0.03)	1.33 (0.09)	41
1000–10000	5813 (52)	0.10 (0.04)	0.32 (0.04)	1.11 (0.03)	1.33 (0.08)	24

The usual eccentricity trends can be gleaned from Table 4: short-period planets are tidally circularized, and the range of eccentricities increases with increasing orbital period. At first glance the tabulated mean metallicities seem consistent with the suggestion that metallicity is correlated with orbital period. However, there are still a relatively small number of stars in the short-period bins. Furthermore, if the stars in the first two period bins are combined, then the mean [Fe/H] of stars with planets in 1–100 day orbits is consistent with that of stars in the last two period bins. Indeed, if the fluctuation in mean metallicity in the first two period bins is real, then it demands a parking mechanism that is extremely sensitive to metallicity. With the current number of stars in these two period bins, the more reasonable interpretation is probably that this represents a fluctuation in small number statistics. Figure 15 shows [Fe/H] as a function of orbital period and eccentricity. *No correlations are found between metallicity and orbital period or orbital eccentricity in systems with extrasolar planets.* In all cases, the host stars tend to have high metallicity. It is interesting that planets in the widest orbits still show a positive metallicity correlation. This lack of support for a link between orbital migration and high metallicity further weakens the hypothesis that accretion is responsible for the planet-metallicity correlation.

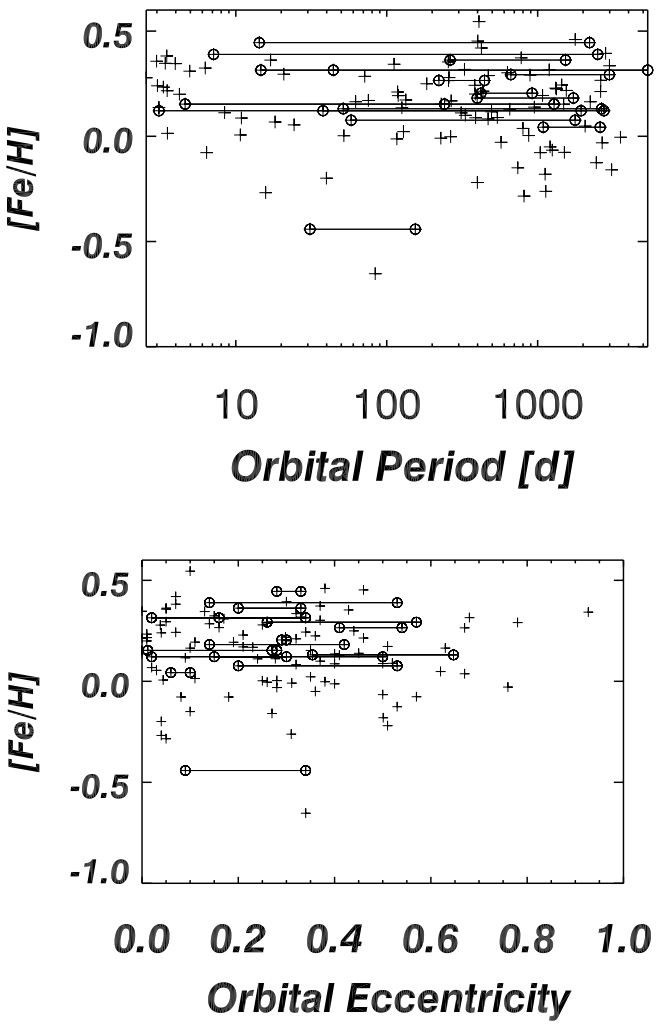

Fig. 15.—*Top:* Orbital periods for 124 exoplanets plotted as a function of stellar metallicity. Multiplanet systems are connected by lines. There is no apparent decline in metallicity with increasing orbital period. *Bottom:* Similarly, orbital eccentricity seems to be uncorrelated with metallicity. In both plots, there is an obvious tendency for multiplanet systems to be found around the highest metallicity stars.

6. DISCUSSION

We have quantified the planet-metallicity relation for stars with extrasolar planets that have velocity amplitudes $K > 30$ m s^{-1} and orbital periods shorter than 4 yr. To enable this analysis, we have carried out a high-precision, uniform spectroscopic analysis of 1040 FGK-type stars in the Keck, Lick, and AAT planet search programs (VF05). A subset of 850 stars was selected that had at least 10 observations spanning more than 4 yr. This requirement on the number and length of observations assures nearly uniform detectability for gas giant planets with orbital periods shorter than 4 yr. We find that the probability of forming a gas giant planet can be expressed as a power law in terms of the number of metal atoms: $\mathcal{P}(\text{planet}) = 0.03[(N_{\rm Fe}/N_{\rm H})/(N_{\rm Fe}/N_{\rm H})_\odot]^2$. Fewer than 3% of stars with subsolar metallicity have detected planets. However, above solar metallicity, there is a smooth and rapid rise in the occurrence of detected gas giant planets as a function of increasing metallicity. In the highest metallicity bins ([Fe/H] $> +0.3$ dex), 25% of the stars have detected gas giant planets.

We find that the ensemble of stars on the planet search surveys are systematically more metal-rich by 0.09 dex than a volume-limited sample of stars. This is likely to be the result of the inclusion of more massive and intrinsically more metal-rich stars in the magnitude-limited sample used by planet hunters. Therefore, a comparison between stars with planets and stars in a volume-limited sample has a built-in bias that inflates the true planet-metallicity correlation. Instead, the spectroscopic analysis presented here is referenced to all stars on the Keck, Lick, and AAT surveys and provides a statistical result that is free of selection effects or detectability biases. Indeed, the fraction of stars with planets in each metallicity bin has not changed over the last year (Fischer et al. 2004) in spite of a revised analysis and the addition of more than 200 stars and a dozen detected planets.

Using Yale isochrone stellar masses, we identify a correlation between stellar mass and metallicity that is likely related to selection biases intrinsic to a magnitude-limited sample. Thus,

stellar mass will also track correlations between stellar metallicity and planets. The data in hand suggest that metallicity, rather than stellar mass, plays the strongest role in the occurrence of planets. At all stellar masses, there is a +0.12 dex offset in the metallicity distribution for stars with planets relative to stars without planets. Expanded surveys of higher mass stars to detect extrasolar planetary systems should still prove valuable in better understanding the separate effects of stellar mass and metallicity. Both factors (high stellar mass and high metallicity) potentially provide more raw materials for planetesimal formation in protoplanetary disks. However, with the data in hand, high stellar metallicity appears to be the best predictor for the presence of a gas giant planet.

We also find that the high metallicity may play a role in the fraction of stars with multiple-planet systems. Among stars with planets, only 1 of 22 stars (4.5%) with subsolar metallicity has a multiple-planet system, compared to 13 of 98 stars (13%) with $[Fe/H] > 0.0$. There is also a tendency for the total detected planet mass to increase with increasing metallicity. As more planetary systems are found orbiting subgiants that have more massive progenitors, it will be interesting to follow these metallicity trends.

The uniformly analyzed Keck, Lick, and AAT data were scrutinized to better understand the origin of the planet-metallicity correlation. If stars with detected gas giant planets are born from high-metallicity molecular clouds, then they should be metal-rich throughout. However, if the stars acquire their high metallicity by accreting gas-depleted material during their late pre–main-sequence or early main-sequence lifetimes, then the mark on the star is quite different: only the CZ is enriched and the underlying layers of the star have lower metallicity. If accretion is responsible for the observed high stellar metallicity for stars with detected planets, then there are several fossil signatures that might be detected:

1. The upper boundary in stellar metallicity should rise as the mass of the convective envelope in main-sequence stars decreases. This effect is not observed.

2. As stars evolve onto the subgiant branch, the convective envelope mixes with deeper layers and the pollution limited to the CZ should be diluted. However, the planet-metallicity correlation persists for subgiants and is quantitatively indistinguishable from the correlation observed for main-sequence stars.

3. Variations might exist in elemental abundances as a function of condensation temperature. Individual abundances measured for Na, Si, Ti, Ni, and Fe (unfortunately, with a relatively narrow range of condensation temperatures) show identical patterns for stars with and without planets.

4. Metallicity could be correlated with orbital parameters, with systems with high eccentricity and short periods showing enhanced accretion signatures. However, even low-eccentricity planets with the longest detected periods orbit metal-rich stars.

Therefore, we conclude that stars with detected gas giant planets are metal-rich throughout their interiors and thus the planet-metallicity correlation is likely to be an outcome of an initial condition rather than acquired pollution. If nearly solar metallicity is required for the formation of gas giant planets, then these types of solar systems would be rare in the early galaxy and an increasingly common occurrence over the last 4–5 Gyr.

It is worth remembering that our solar system would not have been counted in the solar metallicity bin in Figure 5. According to the definitions established for this planet-metallicity correlation, this is exactly as it should be; the Sun does not have a Jupiter-like planet in an orbit that is shorter than 4 yr. Rather, the sun is like 90% of the "planetless" stars in the solar metallicity bin.

We are indebted to Geoff Marcy for a careful reading of this manuscript and excellent suggestions that improved the content. We thank Paul Butler, Geoff Marcy, and Steve Vogt for providing us with high S/N spectra from Keck Observatory that we used in our analysis. We thank Paul Butler, Chris McCarthy, Chris Tinney, Hugh Jones, Alan Penny, and Brad Carter for providing spectra from the Anglo-Australian Telescope. We thank Doug Lin, Greg Laughlin, Klaus Fuhrmann, Norm Murray, Bob Noyes, John Johnson, Jason Wright, and Re'em Sari for helpful discussions. We thank Howard Isaacson for checking the orbital elements in Table 2. We thank the referee, Bob Noyes, for an extraordinarily careful reading and excellent suggestions. We gratefully acknowledge the dedication of the Keck Observatory staff, the Lick Observatory staff, and the AAT Observatory staff. We acknowledge support by NASA grant NAG5-75005 (through G. Marcy) and by Sun Microsystems. We thank the NASA and UC Telescope assignment committees for allocations of telescope time. The authors extend thanks to those of Hawaiian ancestry on whose sacred mountain of Mauna Kea we are privileged to be guests. Without their generous hospitality, the Keck observations presented here would not have been possible. This research has made use of the SIMBAD database, operated at CDS, Strasbourg, France, and the Vienna Atomic Line Database.

REFERENCES

Butler, R. P., Marcy, G. W., Williams, E., McCarthy, C., Dosanjh, P., & Vogt, S. S. 1996, PASP, 108, 500
Cochran, W. D., Hatzes, A. P., & Hancock, T. J. 1991, ApJ, 380, L35
Fischer, D. A., Valenti, J., & Marcy, G. W. 2004, in IAU Symp. 219, Stars as Suns: Activity, Evolution and Planets, ed. A. K. Dupree & A. O. Benz (San Francisco: ASP), 29
Fuhrmann, K., Pfeiffer, M. J., & Bernkopf, J. 1997, A&A, 326, 1081
———. 1998, A&A, 336, 942
Gonzalez, G. 1997, MNRAS, 285, 403
———. 1998, A&A, 334, 221
———. 1999, MNRAS, 308, 447
Gonzalez, G., Laws, C., Tyagi, S., & Reddy, B. E. 2001, AJ, 121, 432
Hillenbrand, L. A., & White, R. J. 2004, ApJ, 604, 741
Kupka, F., Piskunov, N. E., Ryabchikova, T. A., Stempels, H. C., & Weiss, W. W. 1999, A&AS, 138, 119
Kurucz, R. 1993, Kurucz CD-ROM 13, ATLAS 9 Stellar Atmosphere Programs and 2 km/s Grid (Cambridge: SAO)
Kurucz, R., Furenlid, I., Brault, J., & Testerman, L. 1984, Solar Flux Atlas from 296 to 1300 nm, National Solar Observatory Atlas (Sunspot: NSO)
Latham, D., Stefanik, R., Mazeh, T., Mayor, M., & Burki, G. 1989, Nature, 339, 38
Laughlin, G., & Adams, F. 1997, ApJ, 491, L51
Laws, C., Gonzalez, G., Walker, K. M., Tyagi, S., Dodsworth, J., Snider, K., & Suntzeff, N. B. 2003, AJ, 125, 2664
Lin, D. N. C., Bodenheimer, P., & Richardson, D. 1996, Nature, 380, 606
Lodders, K. 2003, ApJ, 591, 1220
Mayor, M., Pepe, F., Queloz, D., Udry, S., Benz, W., Santos, N., & Moutou, C. 2003, Stellar Metallicity and the Formation of Giant Planets—Metal Deficient Stars (Garching: ESO), http://www.eso.org/observing/proposals/gto/harps/4.txt
Murray, N., Chaboyer, B., Arras, P., Hansen, B., & Noyes, R. W. 2001, ApJ, 555, 801
Pinsonneault, M. H., DePoy, D. L., & Coffee, M. 2001, ApJ, 556, L59
Ryabchikova, T. A., Piskunov, N. E., Stempels, H. C., Kupka, F., & Weiss, W. W. 1999, Phys. Scr., T83, 162
Sadakane, K., Ohkubo, M., Takeda, Y., Sato, B., Kambe, E., & Aoki, W. 2002, PASJ, 54, 911
Sandquist, E., Taam, R. E., Lin, D. N. C., & Burkert, A. 1998, ApJ, 506, L65

Santos, N. C., Israelian, G., & Mayor, M. 2000, A&A, 363, 228
———. 2004, A&A, 415, 1153
Santos, N. C., Israelian, G., Mayor, M., Rebolo, R., & Udry, S. 2003, A&A, 398, 363
Sozzetti, A., Latham, D. W., Torres, G., Stefanik, R. P., Boss, A. P., Carney, B. W., & Laird, J. B. 2004, AAS Meeting, 204, 62.01
Udry, S., et al. 2003, A&A, 407, 679
Valenti, J. A., & Fischer, D. 2005, ApJS, submitted (VF50)
Valenti, J. A., & Piskunov, N. E. 1996, A&AS, 118, 595
VandenBerg, D. A., & Clem, J. L. 2003, AJ, 126, 778
Yi, S. K., Kim, Y.-C., & Demarque, P. 2003, ApJS, 144, 259